

Pb-doped p-type Bi_2Se_3 thin films via interfacial engineering

Jisoo Moon[†], Zengle Huang[†], Weida Wu[†], Seongshik Oh^{†}*

[†]Department of Physics and Astronomy, Rutgers, The State University of New Jersey, Piscataway, New Jersey 08854, United States.

*Correspondence should be addressed to ohsean@physics.rutgers.edu and +1 (848) 445-8754 (S.O.)

ABSTRACT: Due to high density of native defects, the prototypical topological insulator (TI), Bi_2Se_3 , is naturally n-type. Although Bi_2Se_3 can be converted into p-type by substituting 2+ ions for Bi, only light elements such as Ca have been so far effective as the compensation dopant. Considering that strong spin-orbit coupling (SOC) is essential for the topological surface states, a light element is undesirable as a dopant, because it weakens the strength of SOC. In this sense, Pb, which is the heaviest 2+ ion, located right next to Bi in the periodic table, is the most ideal p-type dopant for Bi_2Se_3 . However, Pb-doping has so far failed to achieve p-type Bi_2Se_3 not only in thin films but also in bulk crystals. Here, by utilizing an interface engineering scheme, we have achieved the first Pb-doped p-type Bi_2Se_3 thin films. Furthermore, at heavy Pb-doping, the mobility turns out to be substantially higher than that of Ca-doped samples, indicating that Pb is a less disruptive dopant than Ca. With this SOC-preserving counter-doping scheme, it is now possible to fabricate Bi_2Se_3 samples with tunable Fermi levels without compromising their topological properties.

KEYWORDS. Topological insulator, Bi_2Se_3 , Doping, Interface, Spin-orbit coupling

Bi_2Se_3 is a three dimensional topological insulator (TI) with a large bulk band gap, ~ 0.3 eV, and topologically-protected surface states.¹⁻⁴ Ideally, its Fermi level (E_F) should be at the charge neutral point (so-called Dirac point) of the surface states within the bulk band gap. However, due to high density of n-type native defects, the Fermi levels of common Bi_2Se_3 are always far from the Dirac point and frequently above the bulk conduction band minimum, making the bulk metallic.⁵⁻¹⁰ In order to fully utilize all the intriguing properties of the topological surface states, it is essential to find a way to tune the Fermi level, not only toward the Dirac point but also into the p-regime as well. In case of Bi_2Se_3 , substituting a 2+ ion for Bi^{3+} is one of the most obvious ways to reduce the n-type carriers and move toward the p-regime. As expected, soon after the confirmation of Bi_2Se_3 being a TI, several elements such as Ca^{11} , Mn^{12} and Mg^{13} have been found to do the job and successfully converted otherwise n-type Bi_2Se_3 bulk crystals into p-type. In addition, the use of Ca dopant has allowed Bi_2Se_3 thin films to turn into p-type not only in a relatively thick regime (~ 200 nm) via a complex process¹⁴ but also in the thinnest topological regime (6 QLs).¹⁵ However, considering that Ca is much lighter than Bi and that spin-orbit-coupling (SOC) strength, which grows fast (to the 4th power in a hydrogen-like atom) with increasing atomic numbers, is an essential parameter for topological surface states,¹⁶⁻¹⁸ substituting light elements for Bi could have an undesirable side effect of compromising the topological properties. In this sense, a heavy 2+ ion will be a much more desirable compensation dopant than such a light element as Ca. In particular, Pb, which is located right left of Bi in the periodic table should be the most ideal p-type dopant for Bi. However, Pb-counter-doping turns out to be ineffective in converting n-type Bi_2Se_3 to p-type, not only in thin films but also in bulk crystals.^{19,20}

Recently, however, it was found that utilization of carefully-designed buffer and capping layers can help boost the effectiveness of counter-dopants. This was first demonstrated in Ca-doping of Bi_2Se_3 thin films. Despite well-established p-type Ca-doped Bi_2Se_3 bulk crystals as discussed above, Ca-doped Bi_2Se_3 thin films have long failed to reach the p-regime, and only last year, the problem was solved with an interfacial engineering scheme.¹⁵ Then, more recently, another interfacial engineering scheme has enabled Ti-doping to convert otherwise p-type Sb_2Te_3 thin films into n-type.²¹ Ti is a potential n-type dopant for

Sb^{3+} ion in Sb_2Te_3 . However, it had long failed to reach the n-regime of Sb_2Te_3 until a proper interfacial engineering scheme was developed recently. Here, we show that the interfacial engineering scheme now allows Pb-counter-doping to implement p-type Bi_2Se_3 for the first time in any Bi_2Se_3 samples, either thin films or bulk crystals.

Films were grown on $10 \times 10 \text{ mm}^2$ c-plane (0001) sapphire (Al_2O_3) substrates using molecular beam epitaxy (MBE) in a custom-built UHV system with base pressure below 5×10^{-10} torr. The individual sources of high purity (99.999%) Bi, In, Se, and Pb were evaporated from standard effusion cells during the film growth. Film thickness and Pb-doping levels were determined with Rutherford backscattering spectroscopy and quartz crystal microbalance (QCM). Se flux was maintained at least 10 times higher than those of Bi and In to minimize Se vacancies. DC transport measurements were carried out with the standard Van der Pauw geometry using a cryogenic resistive electromagnet system whose base temperature is 6 K. The Pb-doped Bi_2Se_3 films were grown on $(\text{Bi}_{0.5}\text{In}_{0.5})_2\text{Se}_3$ (BIS in short) buffer layers composed of 20 QLs of $(\text{Bi}_{0.5}\text{In}_{0.5})_2\text{Se}_3$ and In_2Se_3 , respectively, as shown in Figure 1. Since In_2Se_3 develops multiple phases when grown directly on the sapphire substrates, 3 QL Bi_2Se_3 is grown first at 135 °C as a seed layer, followed by 20 QL In_2Se_3 grown at 300 °C and annealing to 600 °C, which evaporates out the Bi_2Se_3 seed layer. Then, we cool it down to 275 °C and deposit 20 QLs of $(\text{Bi}_{0.5}\text{In}_{0.5})_2\text{Se}_3$ and Pb-doped Bi_2Se_3 in sequence. Amorphous Se, approximately 100 nm thick, is deposited at room temperature as a capping layer. More detailed information for the BIS buffer layer growth can be found in Ref. 22.

Figure 2 shows doping-dependent Hall effect data of the 20 QL Pb-doped Bi_2Se_3 films. As the doping concentration increases, the hole dopants compensate for the n-type carriers in the Bi_2Se_3 film, leading to increased negative slopes of the Hall effect curve, implying reduced n-type sheet carrier densities ($n_{2\text{DS}}$), until the doping level reaches 0.05%. As the Pb-doping increases further to 0.072%, the negative slope starts to decrease, indicating that the films starts to have p-type carriers in addition to the majority n-type carriers. A decreasing slope of a Hall effect curve in Bi_2Se_3 as the Fermi level approaches the charge neutral point is a commonly observed behavior both with compensation doping and with gating.^{15,23,24} At

0.1%, the Hall curve becomes almost flat, implying that there exist significant level of electron-hole puddles, spatially varying energy levels near the Dirac point²⁵ which is analogous to similar features in graphene.²⁶⁻
²⁸ At 0.2%, the slope increases to a clear positive value, indicating that the Fermi level has now exited the electron-hole puddle regime and clearly entered the p-regime. Up to 1%, the carrier type remains p-type. However, at much higher doping levels, the carrier type changes back to n-type as shown in the 10% data, and the (n-type) n_{2D} becomes extremely high at 20%. Such a carrier-type reversal behavior at high doping concentrations was previously observed in the Ca-doped Bi_2Se_3 film study,¹⁵ and indicates that there is a solubility limit for any compensation dopant. Beyond a solubility limit, the dopants start to introduce extra defects going beyond simple Bi substitution, and it is well known that almost all defects in Bi_2Se_3 behave as n-type dopants.^{5,6}

The n_{2D} s and mobilities (μ s) extracted from Figure 2 are shown in Figure 3, where $n_{2D} = 1/(e \cdot \text{slope})$ and $\mu = 1/(R_{\text{sheet}} \cdot n_{2D} \cdot e)$. Here the data for 0.1% and 20% are not included because they give orders of magnitude higher - nominal for the former and actual for the latter - n_{2D} s than the others. Figure 3(a) shows what we have quantitatively discussed above with Figure 2 on how the n_{2D} s and their signs change with Pb-doping: n-type up to 0.05%, n-p mixing for 0.072% and 0.1%, p-type up to 1.0%, and finally back to n-type for even higher Pb-doping. The mobility data in Figure 3(b) provide further information. The most notable feature is that the μ s of p-type samples are clearly lower than those of n-type samples, which is consistent with the previous Ca-doped Bi_2Se_3 study.¹⁵ The very fact that the 10% n-type sample exhibits a higher mobility than the sub 1% p-type samples strongly suggests that the higher mobility of n-type than p-type samples should be an intrinsic band structure effect rather than an extrinsic dopant-scattering effect. This is also consistent with the known band structure of Bi_2Se_3 : the surface band structure is much sharper above the Dirac point than below,^{3,9,29-31} thus higher Fermi velocity (or/and lower effective mass) and higher mobility for n-type than p-type. Furthermore, the proximity of the bulk valence band to the Dirac point also leads to more scattering channels, thus lower mobility, for the p-type carriers.

In Figure 4, we present scanning tunneling microscopy (STM) images of Bi_2Se_3 films at two different Pb-doping levels (0.6% and 6%) to probe the level of disorder introduced by the doping process. While the 0.6% sample in Figure 4(a) shows the prototypical triangular-shaped step terraces,³² the 6% sample in Figure 4(b) is filled with more irregular morphology. This clearly indicates that high level of Pb-doping in Bi_2Se_3 is accompanied by disorder, as expected from the transport data above. The zoomed-in images of the 0.6% sample in Figure 4(c-d) exhibit almost uniformly-distributed Pb-dopants. Interestingly, the counted Pb-dopant density, 5.4%, is almost 10 times higher than the nominal concentration of 0.6% estimated by QCM. This implies that there is a strong tendency for Pb-dopants to diffuse out of the bulk of Bi_2Se_3 and stay on the interfaces. Then the actual doping levels of the bulk and interfaces are expected to be substantially different (the former being lower and the latter higher) than the nominal doping level.

Finally, we compare highly Pb- and Ca-doped Bi_2Se_3 thin films in Table 1. For small levels (< 1%), we do not find noticeable differences between the two doping schemes, but at high doping concentrations (> 1%), which inevitably introduces significant disorders, the difference becomes noticeable. Table 1 shows that the impact of disorder is less disruptive with Pb than with Ca doping at high doping. First of all, even with much higher Pb doping, the n_{2D} is slightly lower (1.03×10^{13} vs. 1.50×10^{13} cm^{-2}) than the Ca doping, implying that Pb doping entails fewer defects. Second and more noticeably, the μ is substantially higher (949 vs. 217 $\text{cm}^2/\text{V}\cdot\text{s}$) with Pb doping, implying that defects from the Pb-dopant introduce less scattering centers than those from Ca. Although the lower n_{2D} (fewer defects) may be related to the strong tendency for Pb dopants to diffuse out of the bulk, the higher mobility is likely due to the much stronger SOC strength of Pb than Ca. Strong SOC is a necessary condition for the absence of backscattering for topological surface states, so light dopant like Ca is much more likely to induce backscattering than Pb. Further studies will be needed to fully understand the role of different SOC strengths in compensation-doped topological insulators.

In conclusion, we have achieved the first Pb-doped p-type Bi_2Se_3 system. The key is utilization of the BIS buffer layer in combination with a protective capping layer. It is particularly notable that the

interface engineering scheme enabled access to a doping regime that cannot be accessed in bulk crystals with the same dopant. This is in stark contrast with the Ca-doped Bi_2Se_3 system, for which p-type bulk crystals have long existed before p-type thin films became available with an interface engineering scheme. When compared with Ca doping, Pb-doping has a clear advantage of preserving the strong SOC of the TI system: the much higher mobility of a heavily Pb-doped Bi_2Se_3 than a Ca-doped one seems to support this idea. The ability to control the Fermi level of a TI system without compromising their topological properties will provide new opportunities for engineering topological materials.

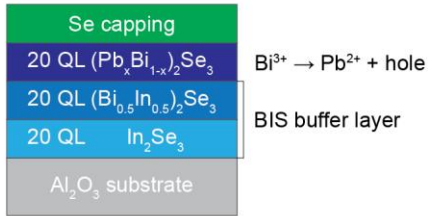


Figure 1. Schematic layer structure of the 20 QL Pb-doped Bi_2Se_3 films. The Pb-doped Bi_2Se_3 is grown on the BIS buffer layer and followed by a Se capping layer. The dopants of Pb^{2+} introduce holes by replacing the Bi^{3+} atoms in the Bi_2Se_3 system. Pb-doping in Bi_2Se_3 films is feasible only on top of the BIS buffer layer scheme in combination with proper capping layers.

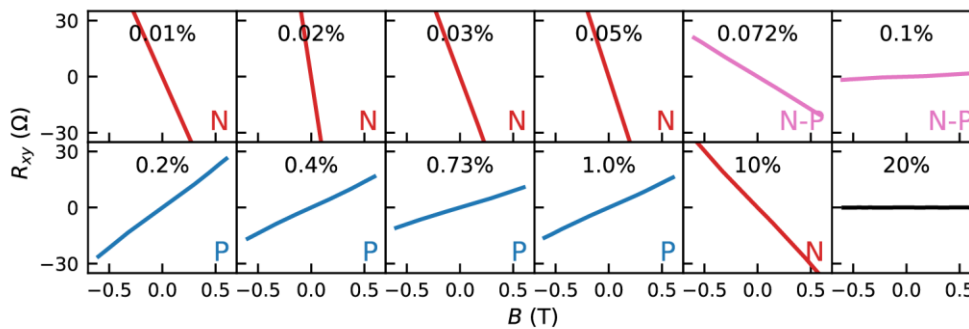


Figure 2. Doping-dependent Hall effect data for the 20 QLs of Pb-doped Bi_2Se_3 films at 6 K. N-type (negative slope), n-p mixing, and p-type (positive slope) curves are colored red, pink, and blue, respectively. The n-regime ranges up to 0.05%. There exists an n-p mixed regime around 0.072 ~ 0.1% between n- and p-type. The 20 QL Pb-doped Bi_2Se_3 film becomes p-type from 0.2% to 1.0%. The carrier type turns back to n-type above 1% as shown in the 10% data. The n_{2D} becomes very high at 20%, thus it is difficult to recognize the carrier type, which is indicated by the nearly flat Hall effect data and colored as black.

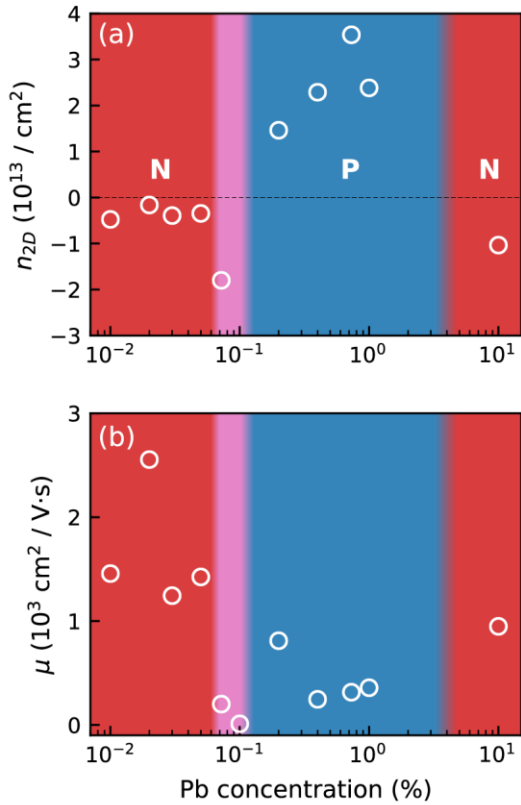


Figure 3. Transport properties of the 20 QL Pb-doped Bi_2Se_3 films. (a) Sheet carrier density and (b) mobility as functions of the Pb doping concentration. Negative and positive n_{2D} data indicate n- and p-type carriers in (a). The n-, n-p, and p-regime are colored by red, pink, and blue, respectively. As the doping concentration increases, the Bi_2Se_3 film undergoes a carrier type transition from n to p passing through a n-p mixing regime. At high concentrations, the film becomes n-type due to disorder beyond the solubility limit of Pb in Bi_2Se_3 , accompanied by a higher (than p-type) mobility shown in (b).

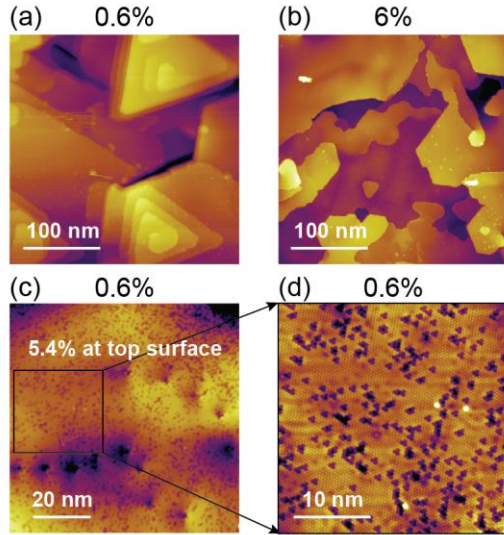


Figure 4. STM images for morphology comparison and doping level investigation at the top surface. (a-b) Top surface topography images of 20 QL Pb-doped Bi₂Se₃ films with (a) 0.6% and (b) 6% of Pb-doping. (c) Zoom-in image in which Pb dopants are visible. (d) Zoom-in image of the area marked by a square in (c). The investigation shows that the concentration of Pb on the top surface is estimated as 5.4%, which is nearly 10 times higher than the nominal concentration of 0.6%.

	n_{2D} (/ cm ²)	μ (cm ² / V·s)
10% of Pb at 6 K	1.03×10^{13}	949
4.4% of Ca at 2 K	1.50×10^{13}	217

Table 1. Comparison of transport properties in 20 QLs of highly Pb- and Ca-doped Bi₂Se₃. The data of Ca-doped Bi₂Se₃ are taken from Ref. 15. The mobility of Pb-doped film is substantially higher than that of Ca-doped one, which means that Pb-doping is less disruptive than Ca-doping in Bi₂Se₃.

REFERENCES

- (1) Hsieh, D.; Qian, D.; Wray, L.; Xia, Y.; Hor, Y. S.; Cava, R. J.; Hasan, M. Z. A Topological Dirac Insulator in a Quantum Spin Hall Phase. *Nature* **2008**, *452* (7190), 970–974.
- (2) Zhang, H.; Liu, C.-X.; Qi, X.-L.; Dai, X.; Fang, Z.; Zhang, S.-C. Topological Insulators in Bi_2Se_3 , Bi_2Te_3 and Sb_2Te_3 with a Single Dirac Cone on the Surface. *Nat. Phys.* **2009**, *5* (6), 438–442.
- (3) Xia, Y.; Qian, D.; Hsieh, D.; Wray, L.; Pal, A.; Lin, H.; Bansil, A.; Grauer, D.; Hor, Y. S.; Cava, R. J.; et al. Observation of a Large-Gap Topological-Insulator Class with a Single Dirac Cone on the Surface. *Nat. Phys.* **2009**, *5* (6), 398–402.
- (4) Hor, Y. S.; Roushan, P.; Beidenkopf, H.; Seo, J.; Qu, D.; Checkelsky, J. G.; Wray, L. A.; Hsieh, D.; Xia, Y.; Xu, S. Y.; et al. Development of Ferromagnetism in the Doped Topological Insulator $\text{Bi}_{2-x}\text{MnxTe}_3$. *Phys. Rev. B* **2010**, *81* (19), 195203.
- (5) West, D.; Sun, Y. Y.; Wang, H.; Bang, J.; Zhang, S. B. Native Defects in Second-Generation Topological Insulators: Effect of Spin-Orbit Interaction on Bi_2Se_3 . *Phys. Rev. B* **2012**, *86* (12), 121201(R).
- (6) Dai, J.; West, D.; Wang, X.; Wang, Y.; Kwok, D.; Cheong, S. W.; Zhang, S. B.; Wu, W. Toward the Intrinsic Limit of the Topological Insulator Bi_2Se_3 . *Phys. Rev. Lett.* **2016**, *117* (10), 106401.
- (7) Tsipas, P.; Xenogiannopoulou, E.; Kassavetis, S.; Tsoutsou, D.; Golias, E.; Bazioti, C.; P. Dimitrakopoulos, G.; Komninou, P.; Liang, H.; Caymax, M.; et al. Observation of Surface Dirac Cone in High-Quality Ultrathin Epitaxial Bi_2Se_3 Topological Insulator on $\text{AlN}(0001)$ Dielectric. *ACS Nano* **2014**, *8* (7), 6614–6619.
- (8) Yilmaz, T.; Hines, W.; Sun, F.-C.; Pletikosić, I.; Budnick, J.; Valla, T.; Sinkovic, B. Distinct Effects of Cr Bulk Doping and Surface Deposition on the Chemical Environment and Electronic Structure of the Topological Insulator Bi_2Se_3 . *Appl. Surf. Sci.* **2017**, *407*, 371–378.
- (9) Pan, Z.-H.; Vescovo, E.; Fedorov, A. V.; Gardner, D.; Lee, Y. S.; Chu, S.; Gu, G. D.; Valla, T. Electronic Structure of the Topological Insulator Bi_2Se_3 Using Angle-Resolved Photoemission Spectroscopy: Evidence for a Nearly Full Surface Spin Polarization. *Phys. Rev. Lett.* **2011**, *106* (25), 257004.
- (10) He, L.; Xiu, F.; Yu, X.; Teague, M.; Jiang, W.; Fan, Y.; Kou, X.; Lang, M.; Wang, Y.; Huang, G.; et al. Surface-Dominated Conduction in a 6 nm Thick Bi_2Se_3 Thin Film. *Nano Lett.* **2012**, *12* (3), 1486–1490.
- (11) Hor, Y. S.; Richardella, A.; Roushan, P.; Xia, Y.; Checkelsky, J. G.; Yazdani, A.; Hasan, M. Z.; Ong, N. P.; Cava, R. J. P-Type Bi_2Se_3 for Topological Insulator and Low-Temperature Thermoelectric Applications. *Phys. Rev. B* **2009**, *79* (19), 195208.
- (12) Choi, Y. H.; Jo, N. H.; Lee, K. J.; Lee, H. W.; Jo, Y. H.; Kajino, J.; Takabatake, T.; Ko, K. T.; Park, J. H.; Jung, M. H. Simple Tuning of Carrier Type in Topological Insulator Bi_2Se_3 by Mn Doping. *Appl. Phys. Lett.* **2012**, *101* (15), 152103.
- (13) Androulakis, J.; Beciragic, E. Robust P-Type Behavior in Polycrystalline, Ball-Milled, Magnesium-Doped Bi_2Se_3 . *Solid State Commun.* **2013**, *173*, 5–8.

- (14) Sharma, P. A.; Lima Sharma, A. L.; Hekmaty, M.; Hattar, K.; Stavila, V.; Goeke, R.; Erickson, K.; Medlin, D. L.; Brahlek, M.; Koirala, N.; et al. Ion Beam Modification of Topological Insulator Bismuth Selenide. *Appl. Phys. Lett.* **2014**, *105* (24), 242106.
- (15) Moon, J.; Koirala, N.; Salehi, M.; Zhang, W.; Wu, W.; Oh, S. Solution to the Hole-Doping Problem and Tunable Quantum Hall Effect in Bi₂Se₃ Thin Films. *Nano Lett.* **2018**, *18* (2), 820–826.
- (16) Moore, J. E. The Birth of Topological Insulators. *Nature* **2010**, *464* (7286), 194–198.
- (17) Kane, C.; Moore, J. Topological Insulators. *Phys. World* **2011**, *24* (02), 32.
- (18) Hasan, M. Z.; Kane, C. L. Colloquium: Topological Insulators. *Rev. Mod. Phys.* **2010**, *82* (4), 3045–3067.
- (19) Kašparová, J.; Drašar, C.; Krejčová, A.; Beneš, L.; Lošt'ák, P.; Chen, W.; Zhou, Z.; Uher, C. N-Type to p-Type Crossover in Quaternary Bi_xSb_yPb_zSe₃ Single Crystals. *J. Appl. Phys.* **2005**, *97* (10), 103720.
- (20) Zhang, Y.; Chang, C.-Z.; He, K.; Wang, L.-L.; Chen, X.; Jia, J.-F.; Ma, X.-C.; Xue, Q.-K. Doping Effects of Sb and Pb in Epitaxial Topological Insulator Bi₂Se₃ Thin Films: An *in Situ* Angle-Resolved Photoemission Spectroscopy Study. *Appl. Phys. Lett.* **2010**, *97* (19), 194102.
- (21) Salehi, M.; Shapourian, H.; Rosen, I. T.; Han, M.-G.; Moon, J.; Shibayev, P.; Jain, D.; Goldhaber-Gordon, D.; Oh, S. Quantum-Hall to Insulator Transition in Ultra-Low-Carrier-Density Topological Insulator Films and a Hidden Phase of the Zeroth Landau Level. *Adv. Mater.* **2019**, 1901091.
- (22) Koirala, N.; Brahlek, M.; Salehi, M.; Wu, L.; Dai, J.; Waugh, J.; Nummy, T.; Han, M. G.; Moon, J.; Zhu, Y.; et al. Record Surface State Mobility and Quantum Hall Effect in Topological Insulator Thin Films via Interface Engineering. *Nano Lett.* **2015**, *15* (12), 8245–8249.
- (23) Kim, D.; Syers, P.; Butch, N. P.; Paglione, J.; Fuhrer, M. S. Coherent Topological Transport on the Surface of Bi₂Se₃. *Nat. Commun.* **2013**, *4*, 2040.
- (24) Kim, D.; Cho, S.; Butch, N. P.; Syers, P.; Kirshenbaum, K.; Adam, S.; Paglione, J.; Fuhrer, M. S. Surface Conduction of Topological Dirac Electrons in Bulk Insulating Bi₂Se₃. *Nat. Phys.* **2012**, *8* (6), 459–463.
- (25) Beidenkopf, H.; Roushan, P.; Seo, J.; Gorman, L.; Drozdov, I.; Hor, Y. S.; Cava, R. J.; Yazdani, A. Spatial Fluctuations of Helical Dirac Fermions on the Surface of Topological Insulators. *Nat. Phys.* **2011**, *7* (12), 939–943.
- (26) Martin, J.; Akerman, N.; Ulbricht, G.; Lohmann, T.; Smet, J. H.; von Klitzing, K.; Yacoby, A. Observation of Electron–Hole Puddles in Graphene Using a Scanning Single-Electron Transistor. *Nat. Phys.* **2007**, *4*, 144.
- (27) Zhang, Y.; Brar, V. W.; Girit, C.; Zettl, A.; Crommie, M. F. Origin of Spatial Charge Inhomogeneity in Graphene. *Nat. Phys.* **2009**, *5*, 722.
- (28) Jung, S.; Rutter, G. M.; Klimov, N. N.; Newell, D. B.; Calizo, I.; Hight-Walker, A. R.; Zhitenev, N. B.; Stroscio, J. A. Evolution of Microscopic Localization in Graphene in a Magnetic Field from Scattering Resonances to Quantum Dots. *Nat. Phys.* **2011**, *7*, 245.

- (29) Bianchi, M.; Guan, D.; Bao, S.; Mi, J.; Iversen, B. B.; King, P. D. C.; Hofmann, P. Coexistence of the Topological State and a Two-Dimensional Electron Gas on the Surface of Bi_2Se_3 . *Nat. Commun.* **2010**, *1*, 128.
- (30) Xu, S.-Y.; Neupane, M.; Liu, C.; Zhang, D.; Richardella, A.; Andrew Wray, L.; Alidoust, N.; Leandersson, M.; Balasubramanian, T.; Sánchez-Barriga, J.; et al. Hedgehog Spin Texture and Berry's Phase Tuning in a Magnetic Topological Insulator. *Nat. Phys.* **2012**, *8* (8), 616–622.
- (31) Wray, L. A.; Xu, S.-Y.; Xia, Y.; Hsieh, D.; Fedorov, A. V.; Lin, H.; Bansil, A.; Hor, Y. S.; Cava, R. J.; Hasan, M. Z. How Robust the Topological Properties of Bi_2Se_3 Surface Are : A Topological Insulator Surface under Strong Coulomb, Magnetic and Disorder Perturbations. *Nat. Phys.* **2011**, *7* (1), 14.
- (32) Bansal, N.; Kim, Y. S.; Brahlek, M.; Edrey, E.; Oh, S. Thickness-Independent Transport Channels in Topological Insulator Bi_2Se_3 Thin Films. *Phys. Rev. Lett.* **2012**, *109* (11), 116804.